PREVENTATIVE MAINTENANCE AND FAILURE ANALYSIS OF AIRCRAFT COMPONENTS

Noam Eliaz[1] and Ronald M. Latanision[2]

[1] *Head – Biomaterials and Corrosion Laboratory, Department of Solid Mechanics, Materials and Systems, Tel-Aviv University, Ramat Aviv, Tel-Aviv 69978, ISRAEL; Phone: +972-3-6407384, Fax: +972-3-6407617, e-mail*: neliaz@eng.tau.ac.il

[2] *Principal and Director – Mechanics and Materials, Exponent® Failure Analysis Associates, 21 Strathmore Road, Natick, MA 01760, USA;*
Phone: +1-508-6528560, Fax: +1-508-6471899, e-mail: rlatanision@exponent.com

ABSTRACT

More than 10 years ago, the three major causes of failures in the Israel Air Force were: maintenance (~16% of failures), manufacturing (~14%), and design (~12%). While fatigue (~34%) and overload (~23%) were the two major failure mechanisms, more than 10% of failures were related to corrosion mechanisms. These include stress corrosion cracking, corrosion fatigue, localized corrosion, hot corrosion, uniform corrosion, *etc.* In this presentation, we provide several definitions of important terms related to failure analysis, present a recommended failure analysis protocol, and summarize several case studies of aircraft components that failed due to corrosion-involving mechanisms.

Implementation of routine condition monitoring techniques (such as ferrography) and failure analysis protocols is valuable in preventing failure recurrence. Ferrography is a method for particles isolation on a glass slide, based upon the interaction between an external magnetic field and the magnetic moments of the particles suspended in a flow stream. By quantifying the number and size of captured particles and determining their chemical composition, shape and surface morphology, the origin, mechanism and level of wear may be determined. Here, we briefly review the application of ferrography in monitoring the health of aircraft assemblies.

Keywords: Failure analysis; Preventative maintenance; Ferrography; Corrosion

1. FAILURE DEFINITION, CAUSES AND MECHANISMS

The term *failure* may be defined as the incapability of a material, device, structure or machine to satisfactorily perform its intended function within the specified limits under specified conditions due to, for example, change in dimensions, shape and/or material properties. Although fracture is the first intuitively-thought (catastrophic) failure, the latter can also reflect decrease in reliability or safety that requires repair or replacement. The term *reliability* itself may be defined as the probability that a component or system should perform its function for a specified period of time when used within established operating conditions. *Failure rate* is the actual or expected number of failures for a given type of component in a given time period (or for a given number of operating cycles). Only in the special case when the likelihood of failure remains constant as time passes, does failure rate equal the inverse of the mean time to failure /1,2/.

Failure analysis is the first necessary stage, following failure, in determining the cause/s (and mechanism/s) of failure, so that effective corrective actions can be implemented, and recurrences of the failure can be eliminated (or, at least, minimized). Thus, failure analysis is based upon determination of failure cause, which is made by use of logical reasoning from examination of data, symptoms, available physical evidence, and laboratory results. Failure analysis may have one or more of the following objectives: (1) identification of failure mechanism and failure cause; (2) providing recommendations for prevention of failure recurrence; (3) determination of the real service conditions; (4) judicial aspects; (5) updating of failure theories and feedback systems for future design of items/assemblies. The *corrective action* is a documented change to design, process, procedure or material, which is implemented in order to correct the root cause of a failure or design deficiency. It usually involves more than one alternative, for example: (1) design upgrades to eliminate or reduce the underlying problem; (2) removal of similar components for further studies/inspections; (3) incorporation of predictive condition-based maintenance techniques; (4) changes in quality control procedures; (5)

revision of maintenance and/or operating manuals; (6) training; (7) requirements relaxation; (8) update of databases; and (9) warning /3/.

A common concept in reliability and failure analysis is the "*failure modes and effects analysis*" (*FMEA*). This method examines potential failures in products or processes, and may be used to evaluate risk management priorities for mitigating known threat-vulnerabilities. It helps selecting remedial actions that reduce cumulative impacts of life-cycle consequences (risks) from a systems failure (fault). By adapting hazard tree analysis to facilitate visual learning, this method illustrates connections between multiple contributing causes and cumulative (life-cycle) consequences. The main stage is to make a description of the parts of a system and list the consequences if each part fails, which are then evaluated by three factors: severity (*S*), likelihood (or probability) of occurrence (*P*), and inability of controls to detect it (*D*). Each index ranges from 1 (lowest risk) to 10 (highest risk), and the overall risk of each failure is expressed in terms of the risk priority number (RPN):

$$\text{RPN} = S \times P \times D. \tag{1}$$

The RPN (ranging from 1 to 1,000) is used to prioritize all potential failures in order to decide upon actions leading to risk reduction, usually by reducing the likelihood of occurrence and improving controls for detecting the failure. The FMEA process, originally developed by the US military in 1949 to classify failures "according to their impact on mission success and personnel/equipment safety," is nowadays used in many formal quality systems, such as ISO 16949 /2,4-6/.

A notable discrepancy exists in the literature between various definitions such as failure mode, failure cause and failure mechanism, often leading to a confusion. Therefore, we find it useful to first clarify the meaning of these important terms herein. *Failure mode* is the effect of the failure mechanism, namely the manner of failure, or what was measured/observed as failure symptoms (e.g. a landing gear fails to open, excessive wear or fracture occurs, *etc.*). *Failure cause* is the circumstance that induces or activates a failure (e.g. design weakness, improper manufacturing, assembly and packaging problems, incorrect maintenance, operator mistake, human factors such as vertigo, contamination, end of lifetime, foreign object damage – FOD, *etc.*). *Failure mechanism* is the physical/chemical process that leads to

failure (e.g. fatigue, hydrogen embrittlement, *etc.*) /1,3/.

One of us (NE) served for several years in the Metallurgical Laboratory, which at that time (more than 10 years ago) was one of the labs within the Division of Materials and Failure Analysis of the Israel Air Force (IAF). The distributions of failure causes and failure mechanisms were, at that time, as in Fig. 1a and 1b, respectively. From Fig. 1a it is evident that maintenance, manufacturing and design (in descending order) were the three major causes of failure. In Fig. 1a, the classification "not applicable" means that a

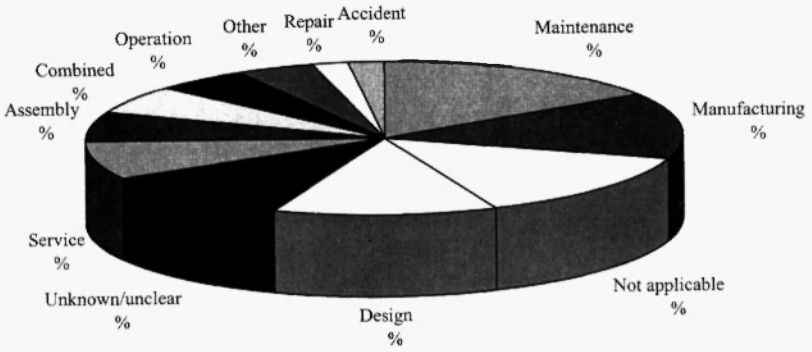

(a)

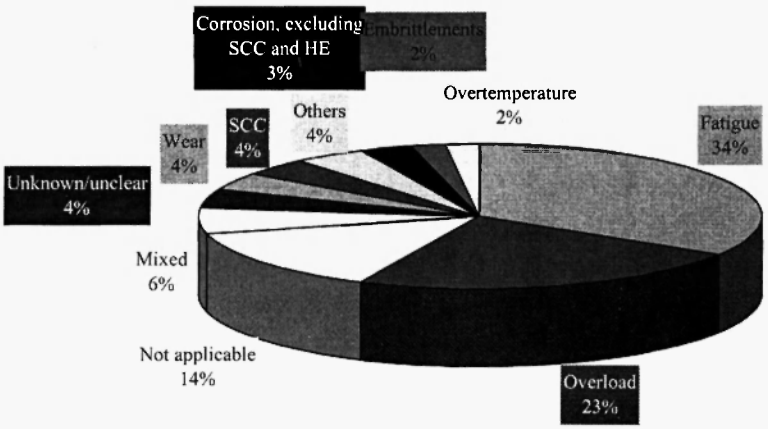

(b)

Fig. 1: Distribution of failure causes and failure mechanisms in the Israel Air Force. Data from more than 10 years ago.

component/system was brought to the lab due to suspects of defects or cracking, but nothing special was actually found. The term "unknown/unclear" reflects a possible situation in failure analysis when the cause of failure cannot be determined unambiguously. The term "other" includes various reasons not contained within the other options in this figure (e.g. electrical short circuit, software error, *etc.*), while the term "combined" means that more than one cause contributed to failure.

Sometimes, the likelihood of a specific failure cause depends on geographic location. One fascinating example is bird migration across Israel and its effect on failures of aircraft in the IAF. Israel is a small country, but strategically located at a junction of three continents. As a result, it is a "bottleneck", into which a large part of the world populations of certain species converge during spring and autumn migration. Over 500 million migrating birds cross the small air space of Israel twice a year. At the same time, the IAF, with its hundreds of aircraft, must train and maneuver and, therefore, finds itself competing with the birds for this very limited air space. According to Newton's Third Law of Motion ("for every action, there is an equal and opposite reaction"), a bird hits the aircraft with the same force as the aircraft hits the bird. In other words, a bird striking a fighter traveling 900 km/h produces approximately 25 tons of impact. Thus, even a small bird can penetrate a fast flying jet like a bullet, downing the aircraft. The IAF, in cooperation with the Society for the Protection of Nature in Israel (SPNI) and Tel-Aviv University, initiated a long-term research program to overcome this complex problem. The leader of this program is Dr. Yossi Leshem, a doctoral student when the program started, and nowadays an internationally renowned birdman. Using advanced radar systems, motorized gliders, drone aircrafts and a liberal number of bird-watchers scattered throughout the nation, Leshem pegged the migration patterns, figuring when bird traffic is the heaviest and at what elevation birds usually fly, depending upon wind and weather conditions. Following collisions between birds and IAF aircraft, bird remains were (and are still) collected from the aircraft or runway. The downy barbules of feathers have specific microscopic structures (similar to finger prints) that enable the identification of the bird even when only minuscule remains are found. Figure 2a shows one of the cartoons used in the IAF campaign to collect feather remains. A 30-min film entitled "Flying with the Birds" was made on this topic and has been broadcasted in 32 countries. From 1984, the research results have been integrated into the IAF flight regulations. Flight training has been coordinated not to clash with the birds.

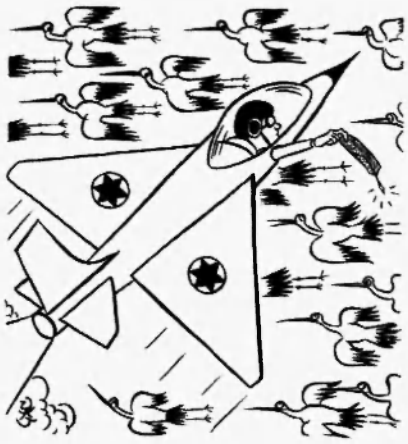

(a)

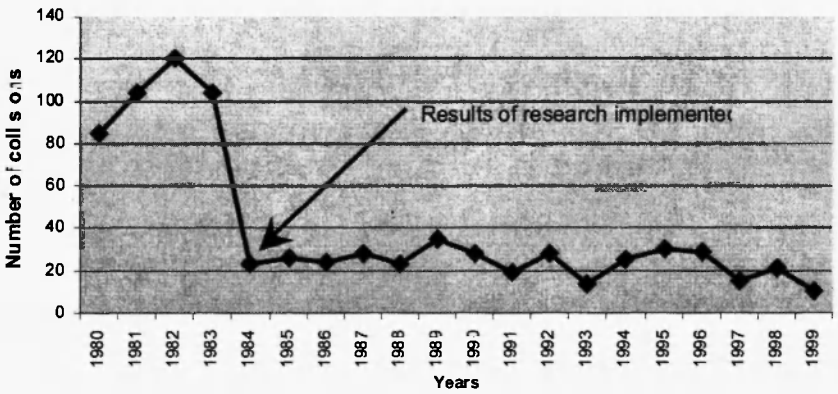

(b)

Fig. 2: (a) A cartoon used in the IAF campaign to collect feather remains after bird-aircraft collisions. (b) The number of air collisions with damage during the previous two decades (1980-1999), before and after implementing Dr. Yossi Leshem's research results /11/.

Bird paths have been analyzed and plotted so IAF pilots would not cross into them. Maps put up in squadron rooms chart the altitudes and migration schedules of birds so that pilots can plot alternate paths, for example fly below or above the buzzards. These new regulations resulted in a reduction of 76% in bird strikes (see Fig. 2b) and have saved the IAF more than 660 million US dollars, not to mention a number of lives. At present, Dr. Leshem is expanding his successful experience with the IAF by creating a global database at the International Center for Study of Migration at Letrun, Israel, to track bird movements and bird strikes in military and civilian aircraft worldwide. The data will be used to estimate the cost of global bird strikes and to develop a regional model of bird movement based on a Geographic Information System. The model is being developed in cooperation with the US Air Force Academy in Colorado Springs, Lockheed Martin and others /7-11/.

In other places worldwide, Bird Strike Committees already exist in several countries, including Italy, Germany and Canada. In the U.S. Air Force, a Bird/Wildlife Aircraft Strike Hazard (BASH) team operates in New Mexico. It has been reported that over 195 people have been killed worldwide as a result of bird strikes since 1988. In addition, from 1990 to 2004, bird and other wildlife strikes cost USA civil aviation over $500 million per year. Over 5,100 bird strikes were reported by the U.S. Air Force, and over 7,100 bird and other wildlife strikes were reported for USA civil aircraft, in 2005 alone. From 1990 to 2004, USA airlines reported 31 incidents in which pilots had to dump fuel to lighten load during a precautionary or emergency landing after striking birds on takeoff or climb /12/.

Figure 1b presents the distribution of failure mechanisms. It is evident that fatigue and overload are, by far, the two major mechanisms identified during failure analyses of aeronautical parts and systems. The meaning of "not applicable" was already explained in regard to failure causes; its percentage is obviously the same for failure causes and mechanisms. By "mixed" mechanisms we refer to synergistic mechanisms such as corrosive wear. Among the corrosion mechanisms, stress corrosion eracking (SCC) was the most common. Hydrogen embrittlement (HE) *per se* is contained within the category "embrittlements" (which also includes mechanisms such as liquid metal embrittlement – LME, tempered martensite embrittlement – TME, *etc.*).

2. FAILURE ANALYSIS PROTOCOL

The failure analysis work resembles handling a puzzle. A successful failure analysis requires expertise, systematic approach, perseverance and, sometimes – luck. Our own experience has taught us that a systematic approach and preservation of knowledge and expertise within the organization may be more valuable than academic/scientific expertise. It is difficult to suggest a general failure analysis protocol. The latter may depend on the specific case and part under investigation, as well as on the personal preferences of the chief investigator. Nevertheless, we present here a suggested model of failure analysis protocol of the type that has been implemented successfully at the IAF.

The failure analysis protocol is based on 12 stages:

1) Collection of background information and samples.
2) Establishment of record keeping.
3) Preliminary inspection of the part/system that failed and documentation.
4) Non-destructive testing (NDT).
5) Selection, identification, cleaning and preservation of samples related to the failure event.
6) Macroscopic and microscopic examination of fracture surfaces (fractography).
7) Microscopic examination of specimens, e.g. in perpendicular to the fracture surface (metallographic cross-sections).
8) Chemical analysis.
9) Mechanical testing.
10) Determination of failure mechanism.
11) Experiments and/or computer modeling to support the suggested failure mechanism.
12) Analysis of all data, formulation of conclusions and recommendations (final report).

In stage #1, information such as history of similar failures, frequency of failure, recent repairs or maintenance documents, the function of the failed item, manufacturing folders (including drawings), operating and maintenance manuals, documentation of the failure event (including evidence of operator), failure mode, *etc.* should be collected. In addition, a careful collection of samples from the site of failure should be made. One should avoid re-assembling of opposite fracture surfaces as this might cause wear and

smearing of morphological and chemical features that are important for the determination of failure mechanism. If corrosion-related failure is suspected, it is advisable to collect liquids that had been in contact with the failed part.

In stage #2, it is important that record keeping be accomplished in an organized manner. This would help the management of the failure analysis work, which is often divided between several labs (or "subcontractors"), as well as the long-term storage of samples. It should also be kept in mind that the findings might eventually lead to legal acts. Therefore, each step should be clearly documented. The aircraft identification number (or name) should be written together with the part/assembly name and the customer who orders the investigation. The place, date and time of sample collection should be noted, together with the personnel in charge of the investigation. In addition, the degree of urgency and the deadline for completion of the investigation are typically noted.

In stage #3, preliminary inspection of the part/system that failed should be carried out. This includes documentation of manufacturing marks on samples, change in shape or dimensions, change in color, evidence for local damage, origin of failure, secondary cracking, evidence for corrosion and/or wear, *etc.* Pictures are usually taken in this stage by means of a digital camera, Polaroid camera, *etc.* Attention should be paid to the direction of light so that important features would be clearly distinguished. A scale bar should be included whenever possible.

In stage #4, non-destructive testing (NDT) may be applied, searching for flaws either at the surface or in the bulk of the material/item. This kind of testing is also known as non-destructive evaluation (NDE) or non-destructive inspection (NDI). Techniques such as magnetic particle testing (MPI) for surface and near-surface flaws in ferrous materials, eddy-current testing (EDT) for surface and near-surface flaws in conducting materials (even coated ones), ultrasonic inspection (UT) for internal flaws and with high sensitivity, liquid penetrant testing (LPI or FPI) for surface-breaking flaws in any uncoated material, acoustic emission (AE) testing, infrared and thermal testing (IR), X-ray radiographic testing (RT) for internal flaws in metallic materials, neutron radiographic testing (NR) for non-metallic materials, *etc.*

In stage #5, the samples important for characterization are selected and clearly identified. All pieces of samples should be marked. Non-soluble ink should be used on all tags. If fluids are present, the samples should be sealed in glass jars. Fracture surface cleaning can be carried out by different techniques, such as acetate film replication, plasma etching, soft rubber, or

mild acids. Samples should be stored in a dry atmosphere, *e.g.* in a desiccator.

In stage #6, macroscopic and microscopic examination of fracture surfaces (fractography) is carried out by means of naked eye, magnifying glass, stereomicroscope, and scanning electron microscope (SEM). Nowadays, the environmental SEM (ESEM™) allows for characterizing non-conducting, dirty or degassing materials without the need for precoating with gold or carbon, which might limit the possibility for local chemical analysis. A sketch of each fracture surface is usually drawn, on which the fracture origin (if identified), important morphological features, expected orientation of applied forces, *etc.* are marked.

Stage #7 provides complementary metallographic information. This may include, but is not limited to, inclusions content, grain size, thickness of surface layers and coatings, defects in vicinity to the fracture surface, secondary cracking, the path of cracking/fracture (*i.e.* intergranular or transgranular), local micro- or nano-hardness testing, *etc.* A correlation between material selection and processing and failure is sought.

Chemical analysis (stage #8) can be performed on the fracture surface itself, as well as on specimens cut from the failed item or on control specimens. There are many analytical techniques available, including arc/spark spectrometry, semi-quantitative energy dispersive spectroscopy (EDS), energy dispersive X-ray fluorescence (ED-XRF) spectroscopy, Auger electron spectroscopy (AES) and X-ray photoelectron spectroscopy (XPS), carbon/sulfur analysis, hydrogen determination, Fourier transform infrared (FTIR) spectroscopy, differential scanning calorimetry (DSC), *etc.* Atomic absorption spectroscopy (AAS) and atomic emission spectroscopy (AES) can be used to determine the concentration of analyte atoms in solution (or in oil).

In stage #9, the short-term mechanical properties should be determined (in particular when a brittle-type failure is suspected). The mechanical testing may be applied to either specimens from the failed part, specimens from similar parts in service, or totally new parts (for control). In the latter two choices, it is preferable that the parts be from the same batch as that of the failed part. Experimental techniques such as tensile, compression, bending, fatigue, impact, creep, fracture toughness or hardness tests may be used.

In stage #10, the failure mechanism is determined. Teams may be utilized to brainstorm possible mechanisms. After all potential mechanisms are listed, a systematic approach should be undertaken to eliminate the ones not leading to the failure.

In stage #11, experimental, mathematical and/or computational approaches are sometimes undertaken to support the suggested failure mechanism. Stress (or structural) analysis can determine the stress in materials and structures subjected to static or dynamic forces or loads. The aim of the analysis is to determine whether the item, assembly or system can safely withstand the specified forces. This is achieved when the determined stress from the applied force(s) is less than the yield strength or ultimate tensile (or compressive) strength – depending on the design criterion and after taking into account a safety factor – that the material can withstand. Experimental techniques may include tension/compression (static), fatigue (dynamic) or fracture mechanics tests to determine the critical crack length and time to failure. Wind tunnels, sensors, *etc.* may be used. Experiments under simulating conditions can be run to distinguish between characteristic fracture morphologies, to determine the expected lifetime of different designs, *etc.* There are three approaches to the structural analysis: the mechanics of materials approach (limited to very simple structural elements under relatively simple loading conditions), the theory of elasticity approach (which is actually a special case of continuum mechanics, and is limited to relatively simple cases, while being mathematically demanding – necessitating the solution of a system of partial differential equations), and the finite element approach. The first two make use of analytical formulation leading to closed-form solutions. The third, actually a numerical method for solving differential equations, is very widely used for structural analysis. Analytical formulations apply mostly to simple linear elastic models, while the finite-element method (FEM) is computer-oriented, applicable to structures of arbitrary size and complexity and to complex loading conditions, with the restriction that there is always some numerical error. FEM can be useful in identifying sites of stress concentrations, distribution of residual stresses, *etc.*

Finally, in stage #12 all data is analyzed, the failure mechanism and failure cause are identified, conclusions regarding the failure event are drawn, and recommendations on routes to prevent failure recurrence are made. A detailed failure analysis report is issued, databases are updated and, if relevant, changes are made in the design ("feedback loop"). We recommend starting the final report with a short abstract (or management summary). We also recommend holding a meeting with all parties involved so that everyone understands the process that was used and the conclusions.

3. CASE STUDIES

In addition to conducting routine failure analyses, organizations such as Air Forces run small and large projects that are aimed at providing tools for future failure analyses and for preventative quality control. Some examples of such projects as well as of failure analyses are described elsewhere for: the study of the effect of manufacturing processes on the fatigue lifetime of aeronautical bolts /13/, hot corrosion in gas turbine components /14/, characteristics of HE, SCC and TME in high-strength steels /15/, failures of bolts in helicopter main rotor drive plate assembly due to improper application of lubricant /16/, and cracking in cargo aircraft main landing gear truck beams due to abusive grinding following chromium plating /17/. An example for the use of finite elements to model the diffusion of hydrogen towards bubbles with cracks and the time-dependent stress intensity factor distribution, so that the time to failure by HE mechanism can be predicted, is also given elsewhere, for a non-aeronautical material /18/. Here, we briefly summarize the results originally published elsewhere /14,17/.

In **case study #1**, failure analyses of two truck beams from the main landing gear (MLG) of a cargo aircraft due to abusive grinding following chromium plating were conducted /17/. The MLG consists of two struts, to which four-wheel bogies are mounted. The landing gear is attached to the wing and is retracted inboard into the thickened juncture of the wing and fuselage. An illustration of the assembly is given in Fig. 3.

The landing gears are being overhauled once in 10 years according to the maintenance instructions of the manufacturer. The main stages in the overhaul process include:

1) Sand cleaning to remove paint and rust.
2) Removal of the chromium plating from marked areas, followed by stress relieve heat treatment.
3) Use of NDT – MPI /19/.
4) Shot peening.
5) Chromium plating of the machined areas per MIL-STD-1501 (class 1, type II) /20/, followed by grinding in accordance with MIL-STD-866B /21/ to restore design dimensions and finish. The chromium plate runout plateau is that area of the chromium-plated surfaces where the chromium thickness changes from the required value to zero. The runout should be produced during the plating operation by use of special electrodes, current robbing, metal tape and shields, to provide a proper gradual runout (over

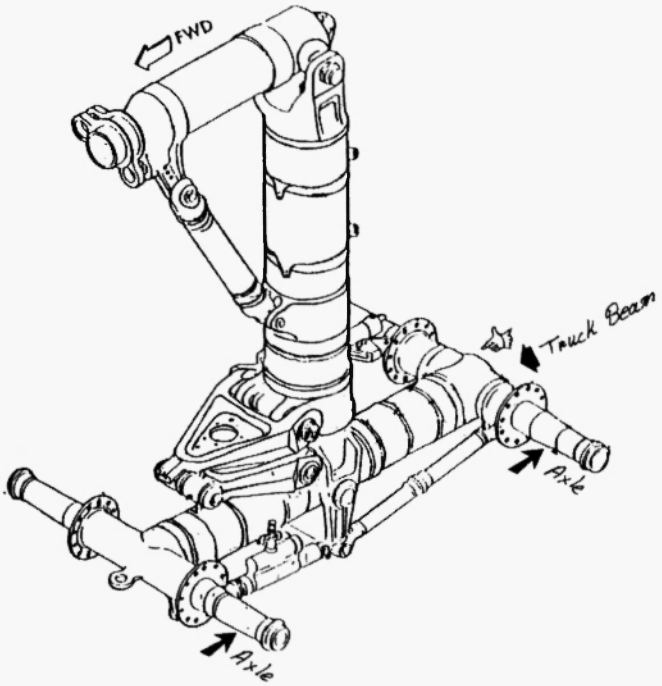

Fig. 3: Illustration of the main landing gear assembly on the subject aircraft. A finger marks the region of failure /17/.

a distance of about 2 mm) without formation of a bead or a square edge. The application of a solid-film lubricant on top of chromium is recommended by the manufacturer, but is not considered as mandatory. Certain users prefer to apply corrosion prevention compounds (CPCs) to the interior of the truck beam after washing.

6) Stress relief heat treatment.
7) Cadmium plating of the rest areas per MIL-STD-870 (type III) /22/, followed by heat treatment to release hydrogen.

In the case study presented herein, while a wheel was being replaced on the subject aircraft, a crack was found on the rear axle bore of the left-hand (L/H) MLG truck beam. One year later, while the same aircraft was being parked, two loud bangs (40 minutes apart) were heard coming from the right-hand (R/H) MLG. The landing gears from both events had been overhauled together. Upon inspection, the R/H truck beam was found cracked longitudinally at two locations on the rear axle bore (Fig. 4). No collapse or collateral damage to other structure resulted. Sections containing crack

fracture surface segments from both truck beams were selected for failure analysis, which included visual examination, NDT, material characterization (namely, chemical analysis, hardness testing and metallography), and analysis of fracture surfaces by SEM/EDS.

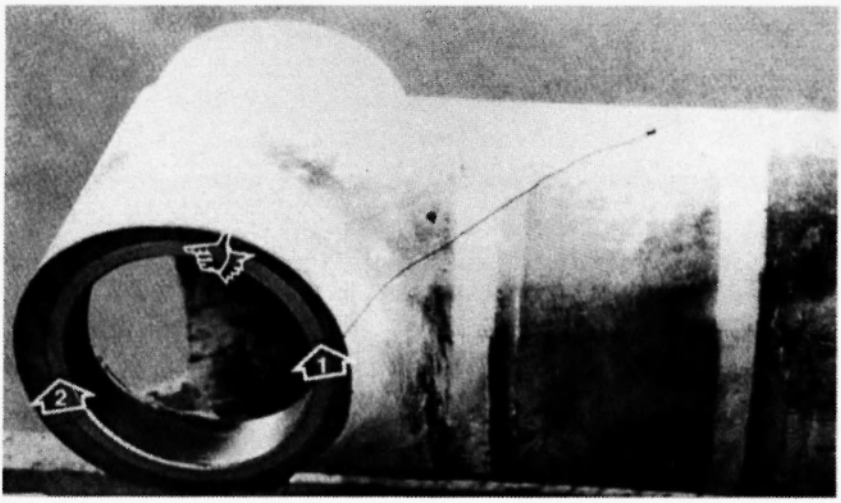

Fig. 4: Macroscopic view of the rear side of the R/H truck beam, revealing two crack origins (marked with arrows), one on each side of the bore /17/.

Visual examination of the R/H truck beam revealed no mechanical damage either in vicinity to the failure region or on the chromium plating. Macroscopic examination of the fracture surfaces revealed ratchet marks propagating from two origins beneath the chromium plating at two opposite locations on the outer wall of the axle (bore). The crack propagation path is shown schematically in Fig. 5. Around the origins, dark brown beachmark patterns were observed (Fig. 6).

The cracks emanating from the two origins in the R/H truck beam (see Fig. 4) were opened in the lab and studied by SEM. Metallographic inspection showed that the chromium plating was nonuniform in thickness, varying between 280 and 120 μm within the runout plateau, where both crack origins were located (Fig. 7). Fractographic observations showed that the crack surface was consisted of two concentric thumbnail-shaped beachmarks zones – an inner small dark zone extending to approximately 0.3 mm from the bore surface, and a surrounding brighter zone extending to nearly 2.5 mm.

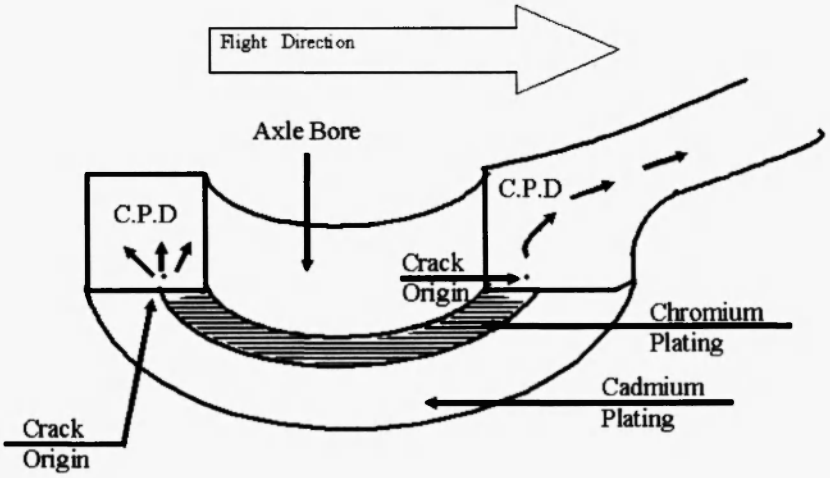

Fig. 5: Scheme of fracture. The chromium-plated zone, crack origins and fracture course are all marked /17/.

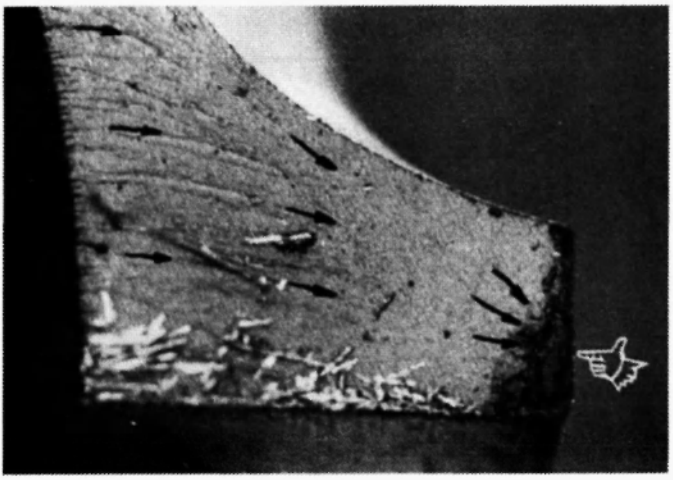

Fig. 6: Stereomicroscope image of the fracture surface around origin 1 from Fig. 4. A dark thumbnail-shaped beachmarks region near the wall is marked with finger /17/.

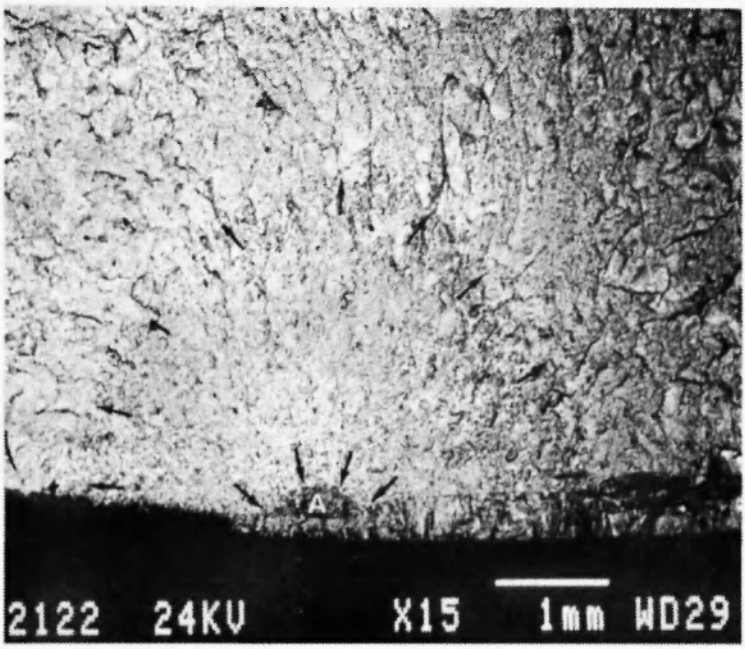

Fig. 7: SEM photomicrograph (back-scattered electrons image) showing origin 2 from Fig. 4 and its surroundings. Two thumbnail-shaped beachmarks zones are marked by arrows. The origin is located within the runout plateau where the chromium layer is thin /17/.

Higher magnification revealed that the inner beachmarks zone was consisted of chemical etching features characteristic of corrosion (Fig. 8). The outer beachmarks zone exhibited a coarse, grainy topography of intergranular separation (Fig. 9). The last portion of the fracture surface (not shown in Fig. 7) was characterized by rupture dimples and quasi-cleavage surfaces characteristic of overload failure.

Thus, it was argued that both cracks initiated from corrosion pits under the chromium plating and propagated in a stable intergranular manner, namely SCC (see Fig. 10). Metallographic cross-section perpendicular to the crack surface through an origin further supported this argument, revealing many pits at the interface between the substrate and the chromium layer, through which cracks propagated within the chromium layer. In some cases, the crack that initiated around the pit penetrated into the substrate as well (see

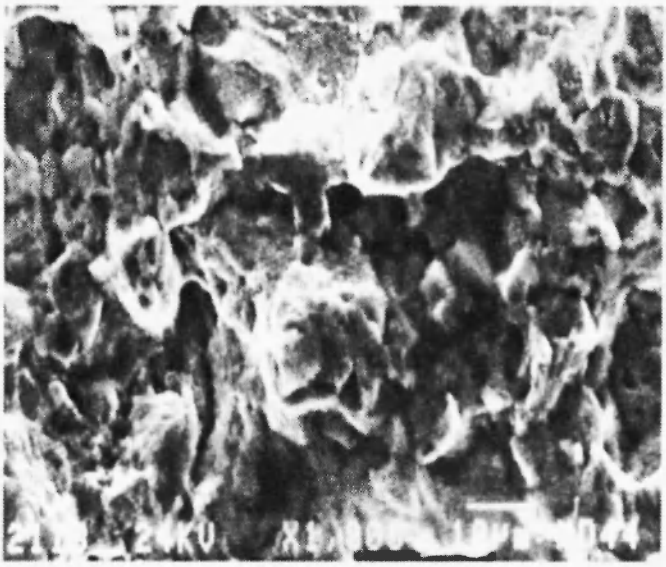

Fig. 8: SEM photomicrograph demonstrating corrosion features within the inner beachmarks zone around origin 1 from Fig. 4 /17/.

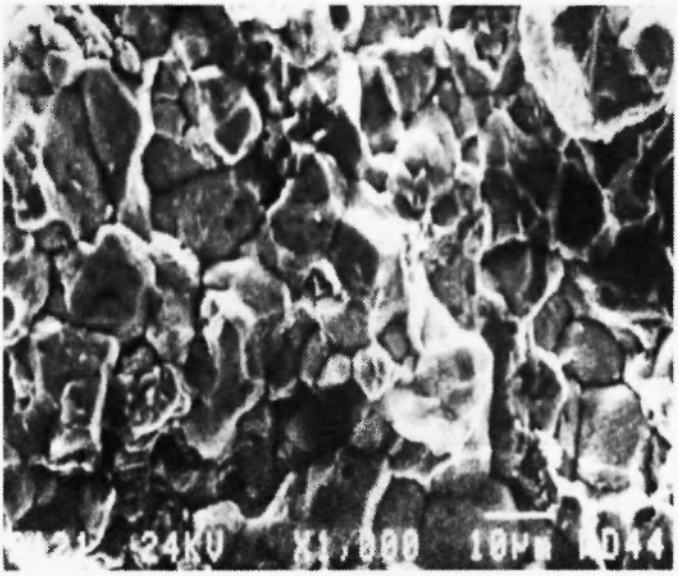

Fig. 9: SEM photomicrograph showing an intergranular fracture morphology within the outer beachmarks zone around origin 1 from Fig. 4. This morphology is typical, among other, to SCC /17/.

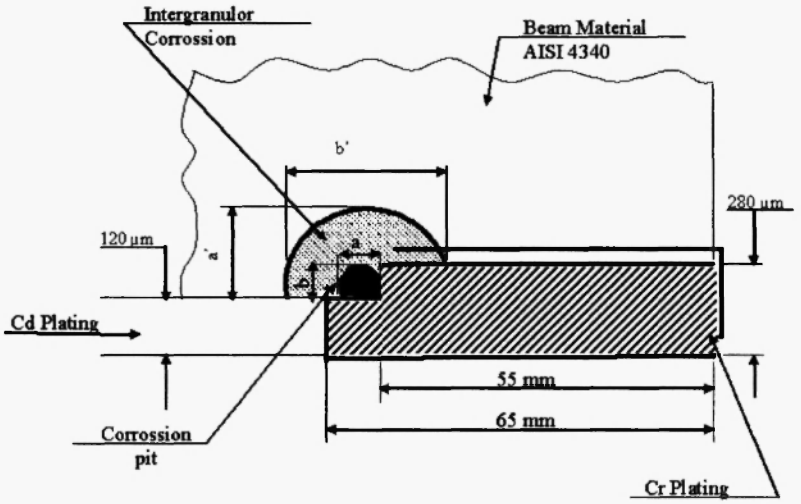

Fig. 10: Scheme of the fracture surface. The area coated with chromium, the corrosion-related pit, and the intergranular corrosion region are shown not in scale /17/.

Fig. 11). Chemical analysis (by means of EDS) at the pit area showed residues of chlorine, which may often be related to corrosion processes. Similar observations were made for the L/H truck beam, in which the crack extended from the outer bearing surface of the axle bore approximately 10.2 cm to the aft end of the longitudinal bore.

In order to better understand the nature of underfilm cracking, the coating was removed around the fracture zone in the R/H truck beam, and Nital etch was carried out in accordance with MIL-STD-867 following fine sand blasting. This revealed already macroscopic areas of overtempered and untempered martensite, indicative of heat damage incurred during abusive grinding (Fig. 12a). These heat-affected areas were located in the chromium plating runout plateau adjacent to the counterbore transition radius, at the edge of the milling (step) zone, and exhibited numerous thermally-induced secondary cracks (Fig. 12b). A similar condition was also observed in the same area on the bearing surface of a peace sectioned from the L/H truck beam specimen. Longitudinal heating marks could be related to the path of the grinding stone on top of the chromium layer. The microstructure of the material in the heat-affected areas and in the area adjacent to the origin of each fracture surface was consistent with overtempered martensite. The

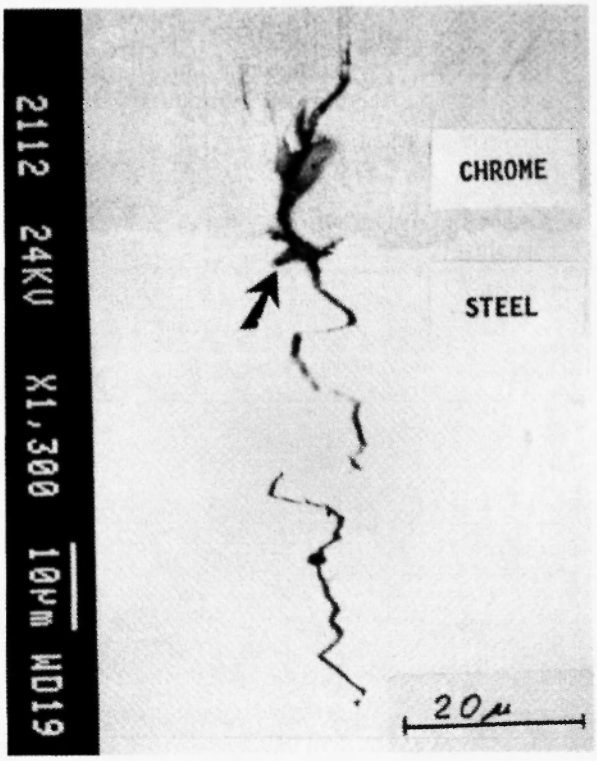

Fig. 11: Microscopic view of an area close to one of the crack origins. The metallographic cross-section was prepared perpendicular to the fracture surface. A secondary crack propagating through the chromium layer into the substrate, in parallel to the fracture surface, is evident. A corrosion pit is evident at the interface between the substrate and the coating /17/.

hardness of the material in these areas was lower than that of the surrounding tempered martensitic structure (Fig. 13).

During grinding much heat is generated, leading to temperature rise which might cause local martensitic transformations, volume increase, increase of residual stresses, and eventually – their release through crack initiation and propagation either into the coating or into the substrate. The high number of cracks and heating marks around the step in the runout plateau indicates that this specific area is very prone to failure as a result of

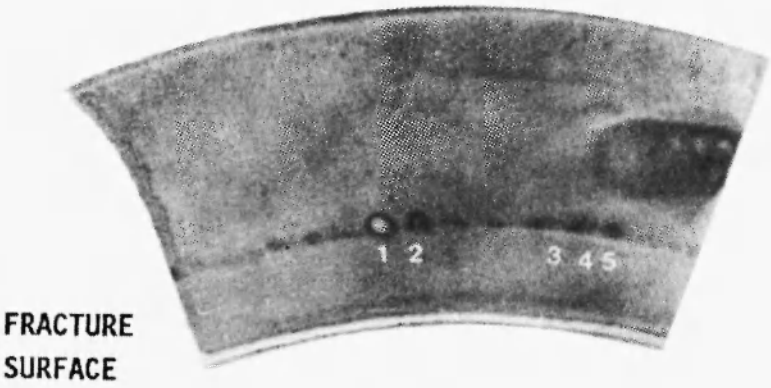

(a)

(b)

Fig. 12: View of the bearing surface of the R/H truck beam specimen. (a) Areas of overtempered and untempered martensite after Nital etch. Magnification ~1.9X. (b) Thermally-induced cracks present in the heat-affected areas revealed by magnetic particle inspection. Magnification ~1.4X /17/.

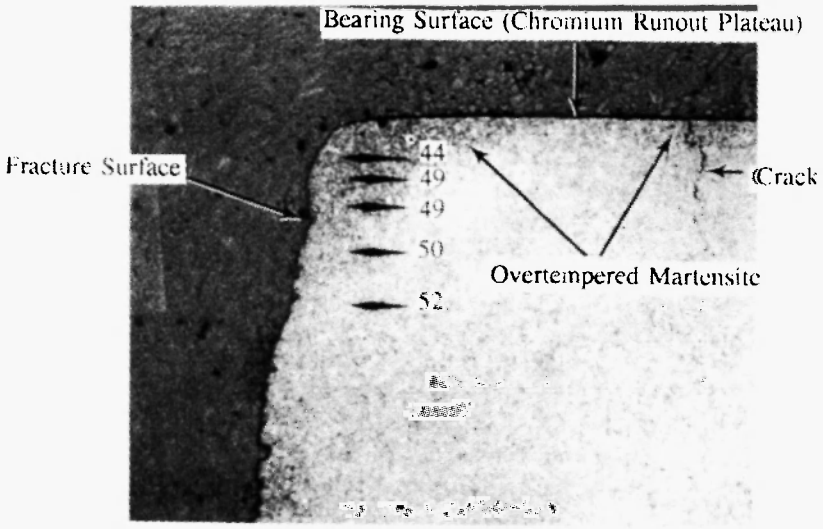

Fig. 13: Photomicrograph showing the overtempered martensitic microstructure (dark area) adjacent to the origin of the fracture surface from the L/H truck beam specimen. Microhardness Knoop measurements (values converted to HRC) were taken in this area and the surrounding normal tempered martensitic structure and are shown to the right of the indentations. Note the crack (arrow) emanating from the bearing surface in a similar overtempered martensitic area. Magnification ~100X /17/.

grinding. The existence of a step may have a twofold effect on the local heating of the substrate. First, edge effects lead to excessive electroplate buildup; thus, more heat is generated during the grinding of the thicker chromium layer at the step region. Second, the heat conduction at a corner is much lower than that in plane. Therefore, the temperature gradient at the step area is relatively high during grinding.

Spectrochemical analysis (*i.e.*, optic emission spectrometry) outside of the heat-affected areas verified that both truck beams were fabricated from the drawing-specified SAE 4340 alloy steel forging. Hardness measurements that were carried out on a cross-section, applying the Vickers method and a load of 10 kg, yielded values within the range 525-536 VHN. These values are equivalent to 51-52 HRC, or an ultimate tensile strength of 264-273 ksi,

which satisfies the drawing requirement for a 260-280 ksi (1.80-1.93 GPa) heat-treat condition. In addition, the rear axle bore outer bearing surfaces of both truck beams were shot peened.

As described before, the identification of beachmark patterns, corrosion products and an intergranular fracture region, are all typical of SCC. Plane strain fracture problems in high-strength materials can be successfully treated by means of fracture mechanics approaches, mainly linear elastic fracture mechanics (LEFM) concepts, which are based on elastic stress field equations. These equations can be used if the size of the plastic zone at the crack tip is small compared to the size of the crack. The stress intensity factor, K, is a measure of the stress and strain environment of the crack. Subcritical flaw growth may occur by SCC. Given a specific material-environment interaction it is found, as in the case of fatigue crack growth, that the SCC rate (and, hence, the time to failure) is governed by K. Similar specimens with the same initial crack but loaded at different levels (*i.e.*, different initial K values) show different times to failure. The specimen initially loaded to the fracture toughness, K_{Ic}, will fail immediately. It should be noted that high-strength materials, like the truck beam steel characterized herein, usually have a low value of fracture toughness. On the other hand, specimens subjected to K values below a certain threshold level, denoted as K_{ISCC}, never fail due to SCC /23/. The SAE 4340 alloy steel is known to have low resistance to uniform corrosion. Furthermore, it is susceptible to SCC in air, particularly in its hardened condition. Electrolyte penetration during service through a cracked coating might lead to formation of corrosion pits around the initial crack tip and to an increase in the stress levels around the pit until K_{ISCC} is attained. Subsequently, the crack will propagate in SCC to the final failure. A literature survey was conducted to determine the crack propagation rate (da/dt) under SCC. While da/dt plots were found for SAE 4340 steel heat treated to 264-273 ksi and exposed to either salt water or deionized (DI) water, no data was found for the more realistic exposure to fresh air. According to the plots that were found, the time necessary to propagate the cracks to failure would be between several hours and days. Yet, in the absence of experimental data for crack propagation under fresh air, no reliable life prediction calculations were carried out for estimation of the time to failure of the truck beams under SCC.

The heating of the substrate during grinding of the chromium plating and the cracking that resulted may be attributed to improper design of the chromium plating structure. The overhaul process typically includes an MPI

after stripping of the chromium coating, and an LPI on the cadmium plate. Nevertheless, it was decided to examine the sensitivity of this technique for chromium plating on the failed beams before coating stripping. Severe fine radial cracking was observed in the region of the thin chromium plating. Moreover, several radial cracks penetrating through the chromium thickness were observed. After stripping of the chromium plating, the failed parts were examined again using the MPI. Radial cracking, similar to that detected by the LPI on top of the coating, was observed. The depth of these cracks was estimated as maximum 0.2 mm by means of the EDT.

In addition to the LPI that is required by the manufacturer, a UT had been developed for early disclosure of beam cracking. However, such a test was carried out one week prior to the second failure event, yielding no warning. Therefore, it was decided to re-examine the effectiveness of this technique too in light of the microscopic findings of the failure analyses. As the crack propagation rate under SCC was unknown, it was decided to consider the maximum pit size observed (0.7 mm) as the size of cracks in the critical stage, or the necessary sensitivity of an effective ultrasonic technique. Indeed, it was found that the UT in use could not identify cracks smaller than 2.5 mm and, therefore, was ineffective.

Based on the information described before, it was **concluded** that cracking of the truck beams initiated near the edge of machined counterbores, around the axle bores. Chromium plating was applied at the counterbores and overlapped the outer edge onto the unmachined areas. The chromium plating was ground flat, a process which introduced high level of burns into the steel beneath the coating. These grinding burns, most likely resulting from thermal heat sink differences along the stepped surface, were probably accompanied by some cracking of the beam metal. Penetration of liquids through radial and "chicken-wire" (mud) cracks in the chromium plating resulted in underfilm pitting corrosion due to the establishment of galvanic coupling between the plating and the truck beam steel. The local corrosion was accelerated by the high cathode-to-anode surface areas ratio in vicinity to a pre-existing microcrack edge. Subsequently, SCC propagated until the cracks reached a critical size, from which rapid failure occurred. When the first crack in the R/H MLG reached a critical size, it failed catastrophically (first loud bang heard). This led to a substantial increase of the stresses acting on the second crack and to its failure (second loud bang heard).

It is worth noting that several years after the failure of the subject aircraft, a similar event was reported by the UK Air Accidents Investigation Branch

(AAIB) /24/. In that case, the right nosewheel stub axle of a Lockheed L1011 Tristar passenger aircraft broke. The failure developed from multi-origin cracking under the chromium plating on the SAE 4340 steel. Crack development had begun in an intergranular mode (SCC or HE), followed by a transgranular (fatigue) mode. The fracture surface had a brown or purple discoloration that was attributed to an enhanced thickness of the iron oxide layer, resulting from overheating after the cracking had begun to develop. Although metallurgical examination did not reveal any microstructural changes that would normally result from overheating during grinding, the manufacturer did detect mud-cracking pattern in the chromium adjacent to the fracture using an etching technique /25/. The manufacturer considered several NDT techniques and concluded that there was none which, in practical terms, could be used in the field to inspect the failure location in the axle. Therefore, the company decided that the only way to ensure that any potential damage is reliably detected is to remove the axle's sleeve and chromium coating at overhaul and perform an ultra-sensitive FPI. Proper revisions were thus incorporated in the Overhaul Manual by June 2000 /24/. This case study implies that similar failures have occurred worldwide in different aircraft, and that it is very important to bring the attention of both designers and overhaulers to the danger in abusive grinding of chromium (and other) plating as well as to the importance of identifying reliable early detection techniques.

Review of both the manufacturer's maintenance instructions and the quality control documentation for the process of chromium electroplating on the failed beams did not indicate any problem. In addition, loading conditions and operating limits were examined. The design load condition was compared to other loads, such as take off, landing and 1 g sustained load while parked. It should be noted that all previous failures of the truck beam occurred while parked under sustained load, and that crack propagation can occur even under very low sustained loads. Under sustained load conditions, the stress around the crack is estimated to be less than 15 ksi, much below the 260 ksi ultimate tensile strength of the steel. Moreover, the location of cracks as observed in the failure analyses would not likely result in the axle separation from the truck and collapse of the gear. Hence, as cracks would likely be detected during a preflight visual inspection, safety of flight or of personnel was not considered as a major concern. Yet, the unacceptable cracking led to the following **recommendations**:

1) Proceed with LPI before every flight until all suspect truck beams would

be replaced.

2) Add an MPI in the chromium region after its stripping, as relevant.
3) Define important NDT parameters previously absent in the maintenance instructions. In addition, define the necessary level of sensitivity as the highest.
4) Apply a routine Nital etch examination of machined chromium regions.
5) Eliminate the step by machining the entire surface instead of counter boring around the axle bore only. Alternatively, expand the counterbore diameter to contain the chromium plating and runout plateau entirely within the flat of the counterbore area.
6) Use a different grinding wheel and take precautions to avoid overheating the material. Add a caution note to start grinding from the point of thickest chromium layer. Specify 75 μm as the minimal thickness of the chromium layer at the edges.
7) Add a primer wipe to the chromium plated surface after grinding to seal all microcracks and those through-thickness cracks not detected by post visual inspection. This may be satisfactory to prevent electrolyte penetration.

In **case study #2** /14/, the macroscopic and microscopic characteristics as well as the proposed mechanisms of Type I (high-temperature) and Type II (low-temperature) hot corrosion were reviewed. Two case histories of gas turbine blade failures were presented, and different practical approaches to minimize hot corrosion were described. The combination of high operating temperatures with aircraft environment that contains contaminants such as sodium, sulfur, vanadium and various halides requires special care to the phenomenon of *hot corrosion*. This phenomenon may be defined as accelerated corrosion, resulting from the presence of salt contaminants such as Na_2SO_4, NaCl and V_2O_5, that combine to form molten deposits, which damage the protective surface oxides. This form of corrosion, unlike oxidation, can consume the material at an unpredictably rapid rate. Consequently, the load-carrying ability of the component is reduced, leading eventually to its catastrophic failure. The inability to either totally prevent hot corrosion or at least detect it at an early stage has resulted in several aircraft accidents, leading to loss of life and/or destruction of engines. At the beginning of the 1990's, a project was initiated at the IAF, aimed towards increasing the awareness of the maintenance teams to the problem of hot corrosion and developing technical instructions to prevent it. Consequently,

failures due to hot corrosion have been minimized, in spite of the relatively aggressive marine environment to which Israeli aircraft is exposed. This is an example where the likelihood of a certain failure mechanism depends on the geographic location, as we have demonstrated for failure causes too.

Figure 14 shows a section of a turbine engine (also known as jet engine). The compressor is located at the exit of the inlet and is marked as *a* in this figure. In the combustor, or burner (*b* in Fig. 14), the compressed air is mixed with fuel and burned. Leaving the combustor, the hot exhaust is passed through the turbine (*c* in Fig. 14), in which the gases are partially expanded through alternate stator and rotor rows. Depending on the engine type, the turbine may be consisted of one or several stages. Like the compressor, the turbine is divided into low-pressure and high-pressure sections, the latter being closer to the combustor. With regard to hot corrosion, several local operating conditions in the engine are important. First, superalloys at turbines serve most time under an oxidizing environment. However, during ignition, a local reducing environment may form due to incomplete burning of fuel. Such a reducing atmosphere can damage the protective surface oxide layer, especially in the presence of contaminants such as Na_2SO_4. Second, hot corrosion is more frequently observed in the low-pressure turbine (LPT) than in the high-pressure turbine (HPT). This is because at the lower temperatures involved in LPT, corrosive contaminants are more likely to accumulate on the surface in significant amounts and/or for a greater percentage of time. Third, hot corrosion is usually greatest at the hottest point on the pressure (concave) surface of the turbine blade; at about midway along the length of the blade, and a short distance back from the leading edge.

Several approaches have been employed to control hot corrosion of gas-turbine components. These approaches include proper selection of structural alloys, application of coatings, washing of hot parts, air filtering, and control

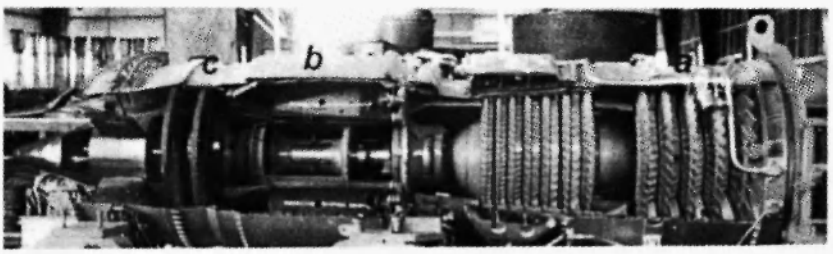

Fig. 14: Section of a gas-turbine engine /14/.

of both fuel cleanliness and composition. Chromium is the most effective alloying element for improving the hot corrosion resistance of superalloys. In order to attain good resistance to high-temperature hot corrosion (HTHC), a minimum of 15 wt.% Cr is often required in nickel-based alloys, and a minimum of 25 wt.% Cr in cobalt-based superalloys. IN 713C, IN 100 and CM 247LC represent the alloys where this criterion is not fulfilled; therefore, they are very susceptible to HTHC. On the other hand, IN 738LC and X-40 have been used to manufacture both stators and rotors. The positive effect of chromium on the HTHC resistance is usually attributed to the reaction of Cr_2O_3 to stabilize the melt chemistry (*e.g.*, by forming a stable Na_2CrO_4 solute), thus preventing dissolution/reprecipitation of the protective oxide scale. The effect of other alloying elements on the hot corrosion resistance of superalloys has been reported as well. Cerium, lanthanum, zirconium, yttrium and scandium significantly increase the resistance as they improve the adhesion between the alloy and the protective oxide. Silicon, platinum, and hafnium have all been shown to have beneficial effects, at least on low-temperature hot corrosion (LTHC) resistance. Titanium, aluminum, and niobium were found to increase the hot corrosion resistance. Cobalt-based superalloys are, in general, more resistant to HTHC than nickel-based superalloys. This may result from the higher melting temperature of Co-Co_4S_3 eutectic (877°C) in comparison to Ni-Ni_3S_2 eutectic (645°C). In addition, the diffusivity of sulfur in cobalt alloys is approximately 100 times lower than in nickel alloys. Cobalt-based superalloys, however, are more susceptible to LTHC than nickel-based alloys. The microstructure of the alloy is another important factor. Secondary phases might lead to an accelerated attack, either along phase boundaries or by selective attack of one phase. In particular, it is important to avoid coarse refractory metal carbides. The use of protective coatings is the preferred approach, even when relatively hot corrosion-resistant base alloys are used. The numerous variants of high-temperature coatings that are in use today may be categorized into three generic types: diffusion (*e.g.*, PWA70, Chromalloy RT22 and Elbar Elcoat 360), overlay (*e.g.*, PWA286 and Co-23Cr-12Al-0.5Y), and thermal barrier coatings (TBC's). Another proven approach to minimize hot corrosion is deluge motoring washes using plain water. This allows for dissolving and carrying away salts and other contaminants, thus preventing the initiation of hot corrosion. Specific washing procedures are usually covered in detail in the relevant maintenance manual for the engine model concerned. Washing may be required either before each flight or up to once a month, depending

on the estimation of the severity of the corrosion environment. An alternative method of establishing wash frequency has been to monitor blade condition using a borescope inspection program, adjusting the wash schedule according to the inspection results. Air filtering is another approach. A limiting level of 0.008 ppm (by weight) has been suggested for the content of Na in the air, below which hot corrosion will not exist. Therefore, secondary protection against hot corrosion may be attained by installation of high-efficiency air filters. Fuel cleanliness affects the initiation and propagation of hot corrosion attack. Hence, the content of the alkali metal, vanadium, and sulfur in the fuel should be carefully controlled. Sometimes, the maximal content of impurities allowed in the fuel is defined as 0.2-0.6 ppm (Na + K), 0.5 ppm V, and 1% S. However, these limits may change if a coating is applied on the blade and/or inhibitors are added to the fuel. Often, additives are added to the fuel; additions of Mg, Cr, Ca, and Ba decrease the corrosion rate. Zinc, added by means of protective coatings or anodes in the fuel tank, is effective in reducing LTHC attack. In the absence of excess NaCl, zinc decreases the solubility of the protective metal oxides in the salt and the electrochemical potential of the corrosion reaction. In the presence of excess NaCl, zinc (rather then other metals from the protective oxide layer) reacts easily with the chloride ion; simultaneously, it serves as a mean of transferring the chloride to the salt-gas interface, where it is transformed to chlorine gas via sulfitation reaction /14/.

One of the case studies of hot corrosion is summarized here. A severely damaged turbine blade was inspected in the lab. Macroscopic inspection indicated the loss of a large piece of blade near the leading edge, at about 1.7 cm from the top of the blade (Fig. 15a). A long crack, about 4.6 mm in length, was found to propagate from this region into the material (Fig. 15b). The crack was then opened at the lab. Inspection of the fracture surface under an SEM revealed fatigue striations, propagating from the leading edge of the blade. Striation analysis indicated the occurrence of high-cycle low-stress fatigue. A transverse metallographic cross-section was prepared through the origin of the crack, perpendicular to the fracture surface, and inspected under an optical microscope. A relatively advanced hot corrosion attack was observed (Fig. 15c), with oxidation penetrating deeply into the blade (up to about 0.8 mm). This high penetration depth, combined with large blisters and eddies within the scale, indicate that the hot corrosion had already progressed to an advanced stage (termed stage 4. In addition, a secondary crack was found to propagate from the scale into the base material, in parallel to the

main fracture surface (Fig. 15d). A similar crack could ultimately propagate to catastrophic failure under fatigue mechanism. SEM/EDS analysis identified the blade material as cast IN 713C, known for its susceptibility to hot corrosion. Based on the aforementioned observations, it was concluded that the blade failed as a result of crack propagation under low stresses of

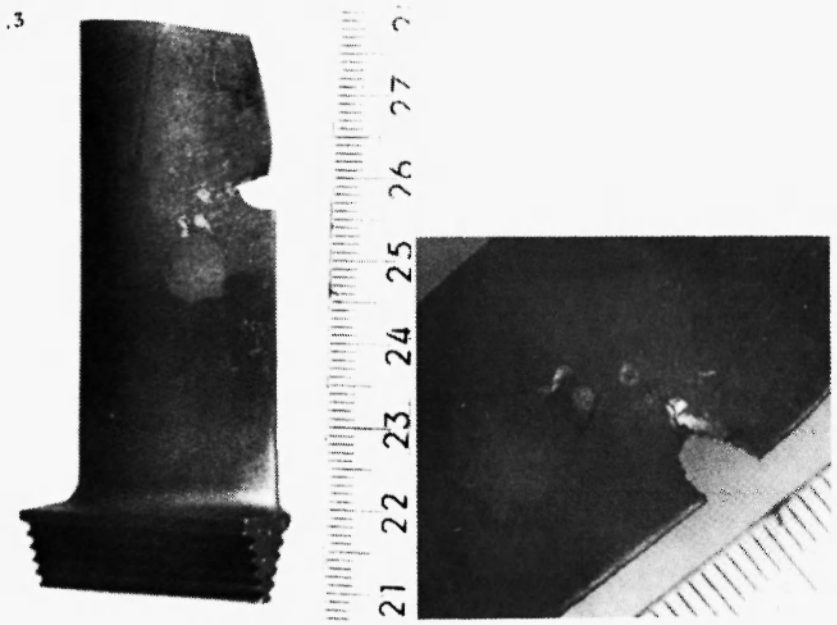

(a) (b)

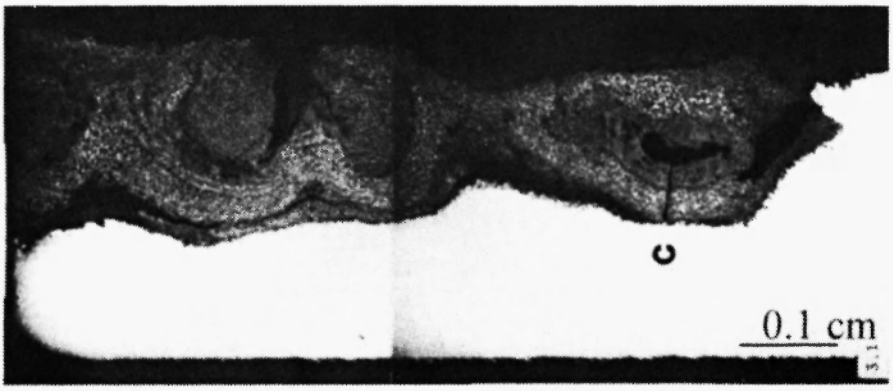

(c)

continued...

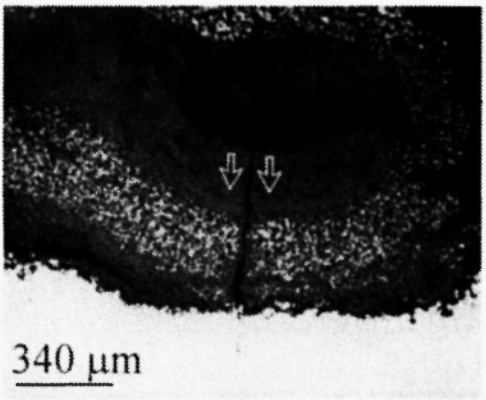

(d)

Fig. 15: (a) Macroscopic view of a turbine blade, indicating the loss of a large piece of material near the leading edge. (b) A crack propagating into the remainder material. (c) Optical micrograph indicating advanced hot corrosion attack. (d) A secondary crack propagating from the scale into the base material, in parallel to the main fracture surface /14/.

vibrations. The origin of the fatigue crack was a preliminary crack (or flaw), formed as a result of advanced hot corrosion attack. Thus, the recommendations of this investigation included replacement of all turbine blades and re-examination of all washing and monitoring operations.

4. CONDITION MONITORING AND FERROGRAPHY

Condition monitoring is the process of monitoring a parameter of condition in machinery, such that a significant change is indicative of a developing failure. It is a major component of *predictive maintenance*, which refers to predictive, periodic and planned maintenance actions taken to maintain a component within design operating conditions and extend its life.

The use of conditional monitoring allows maintenance to be scheduled, or other actions to be taken, in order to avoid the consequences of failure, *before* it occurs. It is typically much more cost effective than allowing the machinery to fail.

Wear is a process in which the surface layers of a solid are ruptured as a result of mechanical action of another body or medium. The act of rupture is localized in a small volume of material, which is removed from the rubbing zone in the form of wear particles. The failure rate of a machine (a "tribosystem") during its lifetime is usually defined by three phases that are evident in a bathtub curve (see Fig. 16): running-in (wearing-in) wear, stationary (normal) wear, and severe (abnormal) wear. Wearing-in occurs during the start-up stages of a new machine, and is therefore also known as "infant mortality." During this phase the quantity of large particles quickly increases, but then settles to an equilibrium concentration during normal running conditions. Machines wearing in an abnormal (*i.e.*, wearing out) mode will produce unusually large amounts of particles and a particle distribution with proportionally more large particles. The different regimes of wear, from mild to severe, are characterized by different size particles, the most severe being associated with particles larger than 1 mm. There are different wear mechanisms, including abrasive, adhesive, surface fatigue, oxidative, fretting, erosion, cavitation, rubbing, cutting, rolling, combined

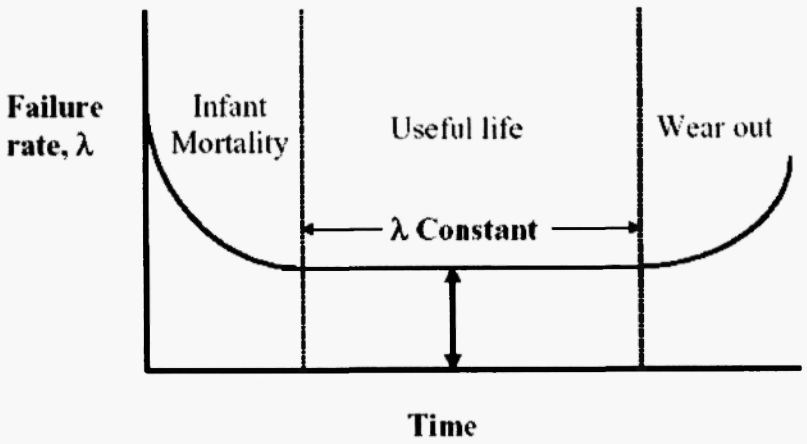

Fig. 16: The Bathtub Curve, illustrating the three stages in the failure (or wear) behavior of a product.

rolling and sliding, and severe sliding wear. However, it is outside the scope of this paper to discuss them in more detail.

Ferrography is an example of condition monitoring technique, which has been found very sensitive and successful in monitoring the wear state of engineering systems, including in aeronautical and aerospace applications. This is a method of particle separation onto a glass slide based upon the interaction between an external magnetic field and the magnetic moments of the particles suspended in a flow stream /26,27/. The method was developed by Westcott and Seifert in the early 1970's to investigate the occurrence of wear particles in lubricated moving components /28-31/, and is used either as the primary analytical method or in conjunction with spectrometric analysis /32/. By quantifying various ferrographic patterns (namely, number, size distribution, texture and shape of wear particles) and determining the composition of different particles on the ferrogram, the origin, mechanism and level of wear can be determined. Ferrography allows prediction of the imminent behavior of the machine. Often, an action may be taken to correct the abnormal wear mode without overhaul (*e.g.*, if abrasive contamination is found, the oil or oil filter may be replaced).

In ferrographic examination, two types of ferrographs may be used. The direct-reading (DR) ferrograph uses optical density to quantitatively measure the concentration of wear particles in a lubricating oil or hydraulic fluid. The particles are subjected to a powerful magnetic-gradient field, and are separated in descending order of size. Light attenuation at two locations along the path – at the entry deposit (DL, large particles) and at a point several millimeters farther down the tube (DS, smaller particles) – is used to quantify the relative concentration DL/DS particles. Values of wear particle concentration (WPC) and the percent of large particles (PLP) are thereby derived, establishing machine wear baselines and trends in wear condition.

The second type of ferrograph, which provides more valuable information, is called an "analytical ferrograph." In analytical ferrography, a ferrogram (*i.e.*, a microscope slide deposited with wear particles) is prepared by pumping a fluid sample that contains wear particles (*e.g.*, oil or diluted grease) through Teflon tubing. The pumping, usually carried out by means of a peristaltic pump, is onto a specially prepared glass substrate, which has a non-wetting barrier painted on one surface to centrally channel the liquid. The ferrogram is slightly tilted, with the entry end elevated, so that the fluid flows downward within the oval-ended barrier to a drain tube that delivers the fluid to a waste bottle (see Fig. 17a). The tilted ferrogram is mounted

above two permanent magnets, which are usually separated by a thin aluminum sheet. The magnets are separated with their magnetic poles counterposed, so that a strong magnetic field gradient is created in the vertical direction above the Al strip. Ferrous particles in the fluid experience a strong downward force. These particles migrate through the fluid down to

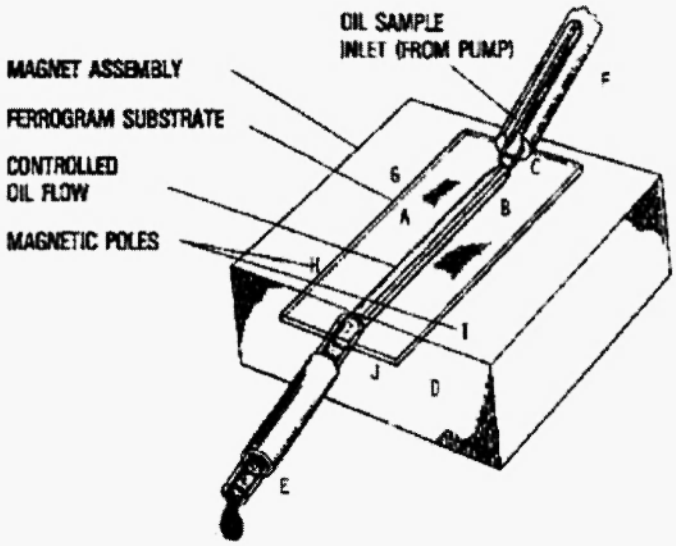

(a)

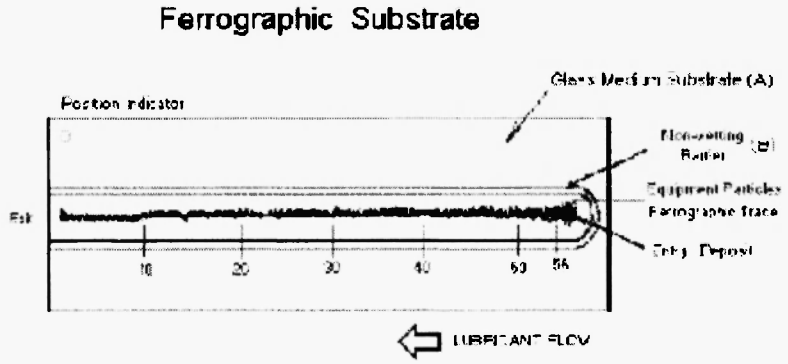

(b)

Fig. 17: The position of the microscope slide on the ferrograph (a) and the resulting ferrogram with deposits of wear particles (b).

the glass surface, where they are deposited in strings perpendicular to the direction of fluid flow. Because the distance from the magnet to the substrate is slightly greater at the entry side than at the exit side, the magnetic field strength is weaker at the entry side, causing only the largest (magnetically affected) particles to deposit. Farther down the ferrogram, the progressively stronger magnetic field deposits progressively smaller particles (see Fig. 17b). Nonferrous particles and contaminants travel downfield in a random distribution pattern, not being oriented by the magnetic field. After all the fluid in a given sample has been run across the ferrogram, a fixer solution is run across the ferrogram to remove residual fluid. After the fixer dries, the ferrogram is ready for observation under the microscope. This is often a special microscope, equipped with both filtered-red reflected and filtered-green transmitted light sources that may be used simultaneously. This lighting scheme, called bichromatic illumination, will show a metal as red and a non-metal as green. Chemical analysis of wear particles can be carried out by means of AES/XPS, EDS, FTIR, *etc.* Heat treatment of the particles on the ferrogram is another quick, inexpensive method of identification. Heating the particles at, for example, 340°C for 90 s yields oxide film thicknesses that are in the range of the wavelengths of visible light. Reflection of light off the metal surface underlying the oxide layer produces interference effects, resulting in coloring of the particles. Different classes of alloys exhibit predictable colors. Therefore, the prior heat history of a particle may sometimes be apparent as temper colors or variations in color of the heat-treated surface. A Wear Particle Atlas was constructed to serve the function of providing information for the identification of various wear particle types, the description of wear modes that generate these particles, and as a guide to the prediction of machine operating condition based on the identified modes /33/. Since then, several new atlases have been published, some of which are in electronic format.

Any ferrographic analysis begins with the sampling procedure, and the validity of a particular analysis depends on how well this procedure is carried out. The ideal sample is taken immediately downstream from the lubricated surfaces. Care is taken to obtain a representative sample by discarding any volume that may have been stagnant in the drain line. The sample is captured in a clean, nonmetallic container, sealed and carefully labeled, including information about lubricant and equipment history. Once in the laboratory, all samples should be brought to a uniform temperature and stirred condition before testing. Machine maintenance records should suggest a proper

sampling frequency. Once a possible problem is detected, the sampling frequency must be increased, until a positive determination is made on machine condition and the action to be taken. For each lubricant parameter that is measured, a control record is built that, after a period of time, will reveal normal operating ranges for a given type of machine/lubricant. Unless parameter operating guidelines are known beforehand, the program must provide enough information to set statistical guidelines for acceptable versus abnormal parameter limits.

Machines already subjected worldwide to ferrographic analysis include gearboxes, bearings, diesel engines, gas turbine engines, gasoline engines, hydraulic systems, compressors, *etc.* Some of the relevant industries include aircraft, naval, automotive, pulp and paper, *etc.* Some typical examples of wear particles generated by different mechanisms and captured by analytical ferrography are shown in Fig. 18 /34/. Ferrography has been applied in the IAF with great success to monitor the health of helicopter gearboxes. However, this work will be covered in another publication.

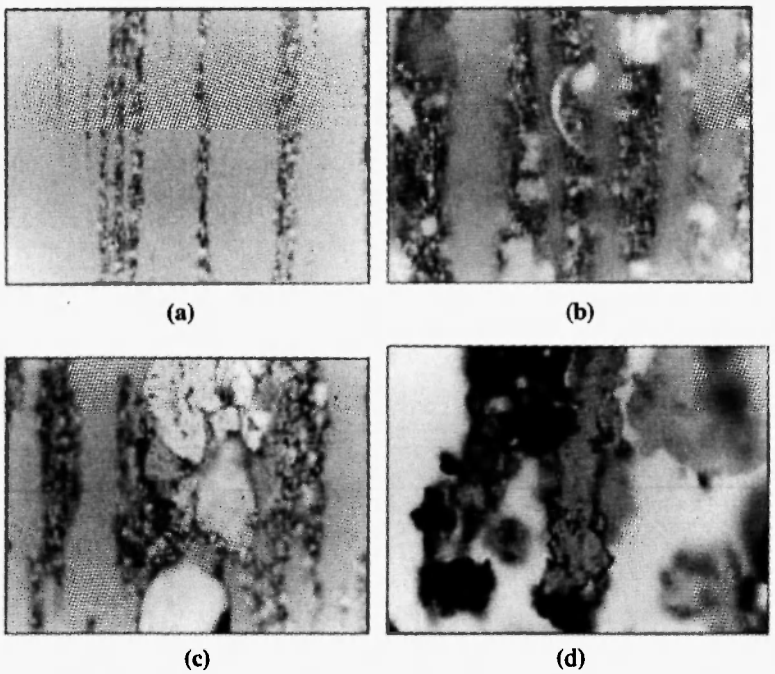

Fig. 18: Typical examples of wear particles that were captured by analytical ferrography. (a) Normal rubbing; (b) Cutting wear; (c) Fatigue platelets; (d) Severe sliding and black oxide /34/.

5. CONCLUDING REMARKS

In this paper we discussed the meaning of several terms often used, sometimes with confusion, in the process of failure analysis. There is obviously a large variety of failure causes and failure mechanisms, which should be examined carefully by the investigator. In order to prevent failure recurrence, the actual cause (or causes) of failure must be identified. Although each investigator brings his/her own expertise and approach, a systematic failure analysis protocol, like the one suggested in this paper, should better be defined and followed precisely. There is great importance in documenting each step of the investigation in much detail as possible, and updating the databases according to the findings so other investigators would be able to take advantage of the experience that has already been gained. Finally, the use of condition monitoring techniques such as analytical ferrography can be very helpful in predicting future failures and preventing them. With the emergence of new technologies every year, important developments can be expected in this field too.

REFERENCES

1. MIL-STD-721C, Definitions of terms for reliability and maintainability.
2. http://en.wikipedia.org
3. MIL-STD-2155 (AS), Failure reporting, analysis and corrective action system.
4. S.J. Uder, R.B. Stone, I.Y. Tumer, "Failure analysis in subsystem design for space missions," in *Proc. 2004 ASME Design Engineering Technical Conferences* (held in Salt Lake City, UT, USA, September 28 – October 2, 2004), DETC2004/DTM-57338 (2004), 1-17.
5. S. Kmenta and K. Ishii, *J. Mech. Design*, **126**(6) (2004), 1027-1035.
6. ISO/TS 16949, Quality management systems: Particular requirements for the application of ISO 9001:2000 for automotive production and relevant service part organizations management systems, 2002.
7. Migrating birds know no boundaries, http://www.birds.org.il.
8. "Flying with the birds," Producer: Benaya Ben Nun, Talia Production, Jerusalem, Israel (1987).
9. http://www.codeonemagazine.com/archives/1999/articles/jul_99/jul4a_99.html

10. Y. Leshem and J. Shamoun-Baranes, "Flight safety, internet and education – a leading tool for global awareness," *Inter. Bird Strike Committee Report IBSC25/WP-OS2*, Amsterdam, April 17-21 (2000).
11. Y. Leshem and E. Sheirmeister, "Birds and flight safety awareness in the Middle East and Africa – A test case," in *Proc. 3rd Joint Annual Meeting Bird Strike Committee USA/Canada* (held in Calgary, AB, Canada), 2001, p. 73-78.
12. Bird Strike Committee USA, http://www.birdstrike.org.
13. S. Ifergane, N. Eliaz, N. Stern, E. Kogan, G. Shemesh, H. Sheinkopf and D. Eliezer, *Eng. Fail. Anal.* **8**(3) (2001), 227-235.
14. N. Eliaz, G. Shemesh and R.M. Latanision, *Eng. Fail. Anal.* **9**(1) (2002), 31-43.
15. N. Eliaz, A. Shachar, B. Tal and D. Eliezer, *Eng. Fail. Anal.* **9**(2) (2002), 167-184.
16. N. Eliaz, G. Gheorghiu, H. Sheinkopf, O. Levi, G. Shemesh, A. Ben-Mordechai and H. Artzi, *Eng. Fail. Anal.* **10**(4) (2003), 443-451.
17. N. Eliaz, H. Sheinkopf, G. Shemesh and H. Artzi, *Eng. Fail. Anal.* **12**(3) (2005), 337-347.
18. N. Eliaz, L. Banks-Sills, D. Ashkenazi and R. Eliasi, *Acta Mater.* **52**(1) (2004), 93-105.
19. MIL-I-6868, Inspection process, magnetic particles.
20. MIL-STD-1501, Chromium plating, low embrittlement, electrodeposition.
21. MIL-STD-866B, Grinding of chrome plated steel and steel parts heat treated to 180,000 psi or over.
22. MIL-STD-870, Cadmium plating, low embrittlement, electrodeposition.
23. D. Broek, *Elementary Engineering Fracture Mechanics*, Martinus Nijhoff Publishers, The Hague, The Netherlands, 1984.
24. Air Accidents Investigation Branch (AAIB) Bulletin, UK Department of Transport (DfT), April 2000.
25. R.W. Messler and R.R. Miller, A new inspection process for detecting abusive grinding damage in hard chromium plated parts, Grumman Aerospace Corp., Airline Plating Forum, 1974.
26. F.E. Lockwood and R. Dalley, Lubricant analysis, in *ASM Handbook, Vol. 18: Friction, Lubrication, and Wear Technology*, ASM International, Materials Park, OH, 1992, pp. 299-312.
27. Staff report, Ferrography: a tool for wear-particle analysis, *Hydraulics & Pneumatics*, November (1986), 59-61.

28. W.W. Seifert and V.C. Westcott, *Wear*, **21** (1972) 27-42.
29. V.C. Westcott, U.S. Patent No. 4,047,814, September 13, 1977.
30. A.A. Reda, R. Bowen and V.C. Westcott, *Wear*, **34** (1975), 261-273.
31. D. Scott, W.W. Seifert and V.C. Westcott, *Sci. Amer.*, **230**(5) (1974), 88-97.
32. J.S. Stecki and B.T. Kuhnell, *Lubr. Eng.*, **41**(8) (1985), 485-493.
33. E.R. Bowen and V.C. Westcott, *Wear Particle Atlas (Revised)*, Vol. 1, Naval Air Engineering Center Contract number N00156-74-C01682, July 1976.
34. B. Bogale, Gear systems – a tribological review, National Tribology Services, Inc. http://www.natrib.com/publications/appnotes/app09.php.